



UNIVERSITY OF LEEDS

This is a repository copy of *Chemical looping Steam reforming of Acetic Acid in a Packed Bed Reactor*.

White Rose Research Online URL for this paper:  
<http://eprints.whiterose.ac.uk/125836/>

Version: Accepted Version

---

**Article:**

Omoniyi, O and Dupont, VAL [orcid.org/0000-0002-3750-0266](https://orcid.org/0000-0002-3750-0266) (2018) Chemical looping Steam reforming of Acetic Acid in a Packed Bed Reactor. *Applied Catalysis B: Environmental*, 226. pp. 258-268. ISSN 0926-3373

<https://doi.org/10.1016/j.apcatb.2017.12.027>

---

© 2017 Elsevier B.V. This manuscript version is made available under the CC-BY-NC-ND 4.0 license <http://creativecommons.org/licenses/by-nc-nd/4.0/>

**Reuse**

Items deposited in White Rose Research Online are protected by copyright, with all rights reserved unless indicated otherwise. They may be downloaded and/or printed for private study, or other acts as permitted by national copyright laws. The publisher or other rights holders may allow further reproduction and re-use of the full text version. This is indicated by the licence information on the White Rose Research Online record for the item.

**Takedown**

If you consider content in White Rose Research Online to be in breach of UK law, please notify us by emailing [eprints@whiterose.ac.uk](mailto:eprints@whiterose.ac.uk) including the URL of the record and the reason for the withdrawal request.



[eprints@whiterose.ac.uk](mailto:eprints@whiterose.ac.uk)  
<https://eprints.whiterose.ac.uk/>

# 1                    **Chemical looping Steam reforming of Acetic Acid in a Packed Bed Reactor**

2    **Oluwafemi A Omoniyi, Valerie Dupont**

3    School of Chemical and Process Engineering, University of Leeds, LS2 9JT, UK.

4    **Keywords**

5    Chemical looping, steam reforming, Acetic acid, Nickel, Hydrogen production

## 6                    **Abstract**

7    Chemical looping steam reforming of acetic acid (CLSR-HAc) was carried out in a packed bed  
8    reactor at 650 °C and 1 atm using two nickel-based catalysts ('A' with alumina support and 'B'  
9    with calcium aluminate support) to study the effect of the temperature of oxidation ( $T_{OX}$ ) on the  
10   efficiency of the process and the materials properties of the catalysts upon cycling. CLSR-HAc  
11   could not be sustained with steady outputs with  $T_{OX}$  of 600°C for catalyst A, but it was conducted  
12   successfully at temperatures up to 800°C, whereas with B it could be operated reaching close to  
13   equilibrium conditions over five cycles with  $T_{OX}$  of 600°C. CLSR-HAc can run efficiently for  
14   further cycles at the right operating conditions ( $S/C$  of 3,  $WHSV$  of 2.5  $hr^{-1}$ ,  $T_{OX}$  800°C,  $T_{SR}$   
15   650°C) even in the presence of the side reactions of acetic acid decomposition and coking. The  
16   yield of hydrogen produced had a minimum efficiency of 89% compared to equilibrium values,  
17   and the acetic acid conversion was in excess of 95% across 10 chemical looping steam reforming  
18   cycles. High purity hydrogen (>90% compared to equilibrium values) was also produced in this  
19   study. Chemigrams obtained from TGA-FTIR analysis indicates that two forms of carbon were  
20   formed on the catalyst during CLSR-HAc; TEM images and diffraction patterns indicate that poly  
21   graphitic carbon and amorphous carbon were formed while SEM images of the oxidised catalyst  
22   showed that the carbon was eliminated during the oxidation step of CLSR. A full carbon elemental  
23   balance of the process confers that majority of the carbon share (ca 90%) was utilised for efficient  
24   steam reforming of acetic acid with ca 10% of the carbon input deposited during the reduction  
25   step and subsequently burned during oxidation over the CLSR cycles.

## 26                    **Abbreviations**

27    CLSR- Chemical Looping Steam Reforming

28    HAc: Acetic acid

29     $T_{OX}$ : Temperature of Oxidation

- 30  $T_{SR}$ : Temperature of Steam reforming
- 31 TGA-FTIR: Thermogravimetric analysis coupled to Fourier transform infrared spectroscopy
- 32 TEM and SEM: Transmission electron microscope and Scanning electron microscope
- 33  $X_{HAc}$  and  $X_{H_2O}$ : Conversion fraction of acetic acid and water respectively
- 34  $\dot{n}_{out,dry}$ : Total molar flow rate dry basis
- 35  $n_i$ : number of moles of specie i
- 36  $y_i$  and  $y_a$ : molar fraction of specie i and all gases in the outlet gas respectively
- 37  $S_{el_i}$ : Selectivity of individual constituent
- 38  $W_i$ : Molar weight of specie i
- 39  $\dot{n}_{i,in}$  and  $\dot{n}_{i,out}$ : molar flow rate in and out of specie I respectively
- 40  $n_{C,gas}$ : Number of moles of carbon gasified in air feed stage
- 41  $n_{Ni,t}$  and  $n_{Ni(i)}$ : Number of moles of nickel oxidised and number of moles of nickel in catalyst
- 42  $(\dot{n}_{Ni \rightarrow NiO})$  and  $(\dot{n}_{C,gas})$ : Rates of nickel oxidation of the reduced catalyst and rate of carbon gasified, respectively
- 43  $X_{Ni \rightarrow NiO}$ ,  $X_{C-gas}$ : Extent of Nickel and Carbon Oxidation
- 44 OC: Oxygen carrier
- 45 sccm: Standard cubic centimeters per minute
- 46 cc/g: cubic centimetre per gram
- 47 CHNS: Carbon, hydrogen and nitrogen elemental analysis
- 48 BET: Brunauer–Emmett–Teller method
- 49 ICP-MS: Inductively coupled plasma mass spectrometry
- 50 TOC: Total Organic Carbon
- 51 S/C: Steam to Carbon ratio

## 52 **1 Introduction**

53 Hydrogen is a gas utilised in many industries globally; it has a global market share of over 40  
 54 million dollars which is expected to increase exponentially to over 180 billion dollars as its  
 55 demand increases[1]. The significant increase in its demand is notably due to its high utilisation  
 56 in industrial applications particularly fertiliser industries, oil refining and petrochemical industries,

57 food processing, metallurgical processes, [1-3] and increasingly due to the growth of fuel cell  
58 technologies. The environmental benefits in regards to its low carbon footprint when utilised  
59 potentially as an energy vector are mitigated by the the fact that 96% of hydrogen consumed  
60 globally is produced from conventional fossil fuels which has prompted vast research on the  
61 utilisation of renewable resources for the production of hydrogen.

62 Biomass resources for H<sub>2</sub> production have advantages over intermittent renewables like wind and  
63 solar in that they are abundant globally, provide a natural storage medium, and because they can  
64 be harnessed easily[4-6]. The production of hydrogen from biomass can be done through different  
65 routes, however; a promising route is an indirect method which involves the fast pyrolysis of the  
66 biomass residue to bio-oil first before its conversion to hydrogen [7]. This method offers  
67 advantages to direct gasification methods on several fronts. Firstly, unlike many gasification  
68 processes, pyrolysis avoids the formation of heavy tars and thus can have a lower burden of clean-  
69 up and maintenance. Secondly, pyrolysis oils can be used for other purposes, particularly as  
70 additives in refining or as feedstock for the production of valuable chemicals. Pyrolysis also  
71 requires milder temperatures than gasification, making the process less prone to the energy  
72 inefficiencies associated with the irreversibilities caused by large temperature gradients in the  
73 system. Finally, pyrolysis operates at lower pressure, thus safer, conditions. Bio-oils are  
74 chemically complex and rather unstable mixtures which has prompted the study on the utilisation  
75 of aqueous fractions of pyrolysis oils, model compounds or mixtures and oxygenates for pilot  
76 scale research and studies [8-15].

77 Acetic acid is one of the most studied model compound of pyrolysis oils for the production of  
78 hydrogen; this is due to its dominant presence in most bio-oil compositions [16, 17]. Its thermal  
79 conversion to hydrogen, however, has been characterised with challenges due to side reactions  
80 and formation of intermediates particularly on the surface of the catalyst [9]. These have increased  
81 the need for process intensification and optimisation measures with the view of reducing some of  
82 the downsides encountered, as well as reducing the energy cost of the process.

83 The conventional process of steam reforming of acetic acid to hydrogen has been well researched  
84 [9, 12, 18-20]. Basagiannis and Verykios concluded that the reforming of acetic acid is  
85 complicated due to side reactions prominent at lower reforming temperatures, they also stipulated  
86 that the rate of carbon deposition observed on the catalyst is generally determined on the reforming  
87 temperature, catalyst utilised and the feed to steam ratio[21].

88 Process intensification measures particularly chemical looping steam reforming (CLSR) has been  
89 promoted to ease the challenges observed in the steam reforming process[22]; CLSR utilises an  
90 ‘oxygen transfer material’ (OTM) also known as ‘oxygen carrier’ (OC) which drives the reactions

91 in a cyclic process as follows. As the steam reforming reactions are very endothermic, heat is  
92 provided at the heart of the process by the oxidation reactions in the reactor under air feed [23].  
93 This ensures no dilution of the reformat mix product with diluent N<sub>2</sub> when the feed flow is  
94 switched to fuel feed and steam, some of fuel being sacrificed first to reduce the OC and thus  
95 activate it as a catalyst of the steam reforming and water gas shift reactions. The use of external  
96 burners to heat up the reformer and the costs associated with the use of highly corrosion resistant  
97 materials and combustion control techniques are thus avoided, while the absence of large  
98 temperature gradients during heat transfer reduces process irreversibilities and thus increases  
99 thermodynamic efficiency. The OC catalyst as utilised in this study should nevertheless have  
100 suitable characteristics particularly a high resistance to attrition, agglomeration and carbon  
101 deposition[24, 25].

102 Previous reported works on the CLSR of acetic acid and other liquids of biomass origin have been  
103 centred on the reactivity of the catalyst across the looping cycles; it has been reported that the fuel  
104 conversion and consequently hydrogen yield reduces upon cycling for the CLSR of bio-diesel and  
105 scrap tyre pyrolysis oils [23, 26]. Other studies indicated that no deterioration occurs in fuel  
106 conversion and hydrogen yield from the CLSR of other liquids of biomass origins investigated  
107 [27-29]. Thus, the efficiency of the fuel conversion and hydrogen yield of CLSR is influenced by  
108 the feedstock and operating conditions utilised, and the deterioration of the reactivity of the  
109 catalyst is generally due to carbon deposition, sintering and thermal decomposition of the  
110 feedstock.

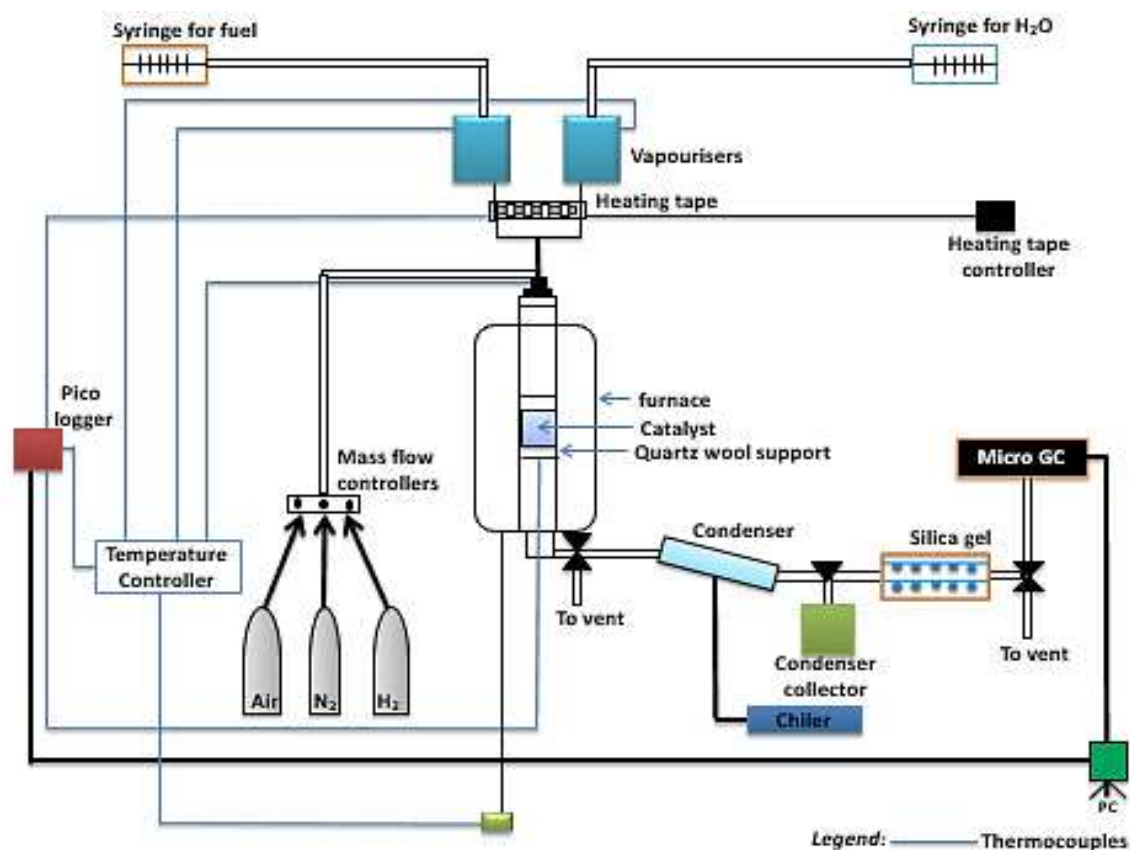
111 This paper studies the redox cycling ability and process efficiency of chemical looping steam  
112 reforming of acetic acid (CLSR-HAc) in a packed bed reactor; ten experimental cycles were  
113 performed using the experimental approach as described in the next section. The auto-reduction  
114 activity of acetic acid of one of the nickel catalyst utilised in the present study has been previously  
115 investigated and it has been established that acetic acid performs considerably well when  
116 compared to the same catalyst after reduction by hydrogen [30]. The process outputs, hydrogen  
117 yield, conversion and selectivity to carbon gases for each cycle and two OC catalysts were  
118 compared with the view to measure consistency across the cycles; and characterisation of the  
119 catalysts was also done post-experimentally to ascertain any changes in morphology. The effect  
120 of the oxidation temperature on the reforming process was examined to ascertain its influence on  
121 the reforming process and full carbon balances were conducted to evaluate the share of solid  
122 carbon by-product during the process.

## 123 2 Experimental approach and methods

### 124 2.1 Materials and reactor set-up

125 Two commercial Nickel-based catalysts were used in this study and were supplied by TST limited;  
126 Catalyst A contained 18 wt. % NiO on alpha-alumina support while Catalyst B contained 15 wt.  
127 % NiO on calcium aluminate support. Both catalysts were supplied as pellets but were crushed  
128 and sieved to 250-350  $\mu\text{m}$  before utilisation. Acetic acid utilised for the experiments was  
129 purchased from Sigma-Aldrich ( $\geq 99\%$ ) and distilled water was used for all experiments.

130 The reactor system utilised in this study, as depicted in Figure 1, is a down flow system using a  
131 fully insulated packed bed reactor consisting of a stainless-steel tube of 12.7 mm internal diameter  
132 and 25 cm length. The reactor was connected to two 180 mm long aluminium and stainless steel  
133 vaporisers; the vaporisers were used to preheat the acetic acid fuel and the water co-reactant  
134 separately before they were introduced into the reactor. For all experimental runs, the pre-heat  
135 temperatures were set at 50°C and 150°C for acetic acid pre-heat and water vaporisation  
136 respectively, this was done to prevent or minimise acetic acid decomposition and induce full water  
137 vaporisation. The temperatures of the vaporisers and the furnace were controlled by a temperature  
138 PID controller while a Pico Log was used to monitor and identify any heat loss in the system. The  
139 flow rates of water and acetic acid was controlled by two separate programmable New Era syringe  
140 pumps while the flow of gasses into the system (air, H<sub>2</sub>, N<sub>2</sub>) were regulated by mass flow  
141 controllers supplied by MKS. The product gas composition were detected and measured by a  
142 Micro gas chromatograph (Micro-GC, Varian) after the effluents passed through a condenser and  
143 a moisture trap; the Micro-GC consisted of two columns, the first which operated with a back  
144 flush was a molecular sieve 5A column and was used to detect H<sub>2</sub>, O<sub>2</sub>, CO, N<sub>2</sub>, while the second  
145 was a Pora Plot Q column used to detect CO<sub>2</sub> and CH<sub>4</sub> as well as C<sub>2</sub> and C<sub>3</sub> gases.



146

147 **Figure 1** Reactor set-up for evaluation of the CLSR-HAc cycles

## 148 2.2 Experimental procedures

149 Chemical looping steam reforming (CLSR) consists of two basic steps; the reducing/ reforming  
 150 step (fuel-steam feed) and the oxidation step (air feed). Both steps as carried out in this study are  
 151 preceded by purging the reactor system with N<sub>2</sub> (200 sccm) and raising the temperature of the  
 152 furnace to the required temperature for each step. The flow rates of acetic acid and water in the  
 153 reducing step was set to 0.978 ml/hr and 1.846 ml/hr respectively and N<sub>2</sub> (27 sccm for experiments  
 154 with WHSV set to 1.18 hr<sup>-1</sup> and 31 sccm for experiments with WHSV set to 2.5 hr<sup>-1</sup>) were also  
 155 utilised in all reforming steps. The reducing/reforming step was carried out at two temperatures:  
 156 600°C and 650°C, and at steam to carbon ratio 3 using 2g of either Catalyst A or Catalyst B. This  
 157 is because previous studies on pyrolysis oils and their model compounds indicated that the  
 158 reforming process is optimal in this range[15, 30-33].

159 The global reactions that are expected to occur in the reducing/reforming step are summarised and  
 160 expressed as follows in Reaction 1 and 2;



163 This includes the auto-reduction of the catalyst by acetic acid (Reaction 1) and complete steam  
164 reforming of acetic acid (Reaction 2). The sequence of reactions for the reducing phase is,  
165 however, more complex than what is described in reaction 1 – 2 as other intermediate and side  
166 reactions might occur. Intermediate reactions might include NiO reduction by CO, H<sub>2</sub> and other  
167 hydrocarbon intermediates, side reactions include coking, formation and dissociation of  
168 intermediates, decomposition of acetic acid, ketonisation and sometimes methanation reactions,  
169 and water gas shift [30].

170 The reducing step for the runs in this study was carried out for 2 hours using 2g of the catalyst.  
171 The catalyst as prepared into granules is first reduced or activated by 5% H<sub>2</sub>/N<sub>2</sub> (Reaction 3) at  
172 the temperature set for the reducing step. Auto-reduction of the catalyst by acetic acid in  
173 subsequent cycles is also carried out after the oxidation step at the temperature set for the reducing  
174 step; this is  $\geq 550^{\circ}\text{C}$  for all experimental runs and has been reported to be adequate for full  
175 reduction of Ni-based catalysts by acetic acid [34].



177 The oxidation step was done at temperatures ranging between 600°C and 800°C with the view to  
178 evaluate the effect of the oxidation temperature ( $T_{\text{Ox}}$ ) on the overall process. Air was passed  
179 through the reactor to re-oxidise the already utilised catalysts from the reducing/reforming step  
180 while also gasifying carbon formed on the catalyst from the preceding fuel feed stage. The main  
181 reactions occurring are summarised in reaction 4-6 and the air feed during the oxidation step was  
182 allowed to run until the concentration of oxygen detected in the micro-GC stabilised at 21 Vol%.



### 186 **2.3 Solids and Condensates characterisation**

187 Characterisation work was also carried out on the used catalyst and collected condensate to analyse  
188 the amounts of carbon and hydrogen deposited over cycles and observe any changes in  
189 morphology after chemical looping steam reforming. The carbon content on the utilised catalyst  
190 was determined using CHNS elemental analysis conducted in a Flash EA 2000 elemental analyser.  
191 BET analysis was conducted using a Quantachrome Nova 2200e instrument to observe any  
192 changes in the open porosity and surface area of the used catalyst. SEM-EDX was conducted using  
193 a high-resolution Hitachi SU8230 and Carl Zeiss EVO MA15 both coupled with an Oxford  
194 Instruments Aztec Energy EDX system, and TEM images was derived using a FEI Tecnai TF20.



195 The SEM-EDX and TEM were carried out for surface topology analysis and solid carbon product  
 196 distribution. TGA-FTIR was also conducted using a Stanton-Redcroft TGA connected to a FTIR  
 197 (Nicolet iS10, Thermo scientific) to observe the mass loss and predict the type of carbon produced  
 198 using the CO<sub>2</sub> chemigram observed. ICP-MS was conducted on the collected condensate using a  
 199 SCIEX Elan 900 by Perkin Elmer and TOC tests were also conducted on the collected condensate  
 200 using a Hach-Lange IL 550 analyser (differential method) to check for possible leaching of the  
 201 catalyst and calculate the carbon content in the condensate respectively.

## 202 2.4 Process outputs and material balances

203 Balances of the N, C, H and O elements during the fuel-steam feed stage and the air feed stage  
 204 were used to determine in turn the reactants conversion to gas products, yield of hydrogen, while  
 205 the gas compositions determined the selectivity to carbon-containing gases as described in [28,  
 206 30, 35]. A nitrogen balance was used to calculate the total molar gas output flow rate ( $\dot{n}_{out,dry}$ )  
 207 using the feed molar rate of N<sub>2</sub> and the molar fraction of N<sub>2</sub> detected by the micro GC ( $\dot{n}_{out,dry} =$   
 208  $\dot{n}_{N_2,in} / y_{N_2}$ ). This in turn was used to calculate the conversion of the reactants in the fuel-steam feed  
 209 stage; acetic acid conversion to gas products in the fuel feed stage is calculated from a carbon  
 210 balance as summarised in Equation 1A while the water conversion (Equation 1B) is calculated  
 211 from a hydrogen balance;

### 212 Equation 1 Conversion (fuel and water)

$$213 X_{HAc}(\%) = 100 \times \frac{(\dot{n}_{out,dry} \times (y_{CO} + y_{CO_2} + y_{CH_4} + 2y_{C_2H_6} + 2y_{C_2H_4} + 3y_{C_3H_6} + 3y_{C_3H_8}))}{2 \times n_{HAc,in}} \quad A$$

$$214 X_{H_2O}(\%) = 100 \times \frac{(\dot{n}_{out,dry} \times (y_{H_2} + 2y_{CH_4} + 3y_{C_2H_6} + 2y_{C_2H_4} + 3y_{C_3H_6} + 4y_{C_3H_8})) - 2 \times n_{HAc,in} \times X_{HAc}}{n_{H_2O,in}} \quad B$$

215 The calculation of the acetic acid conversion to gases did not represent the conversions to solid  
 216 carbon or organic condensates, which were evaluated separately by CHNS analysis of the used  
 217 catalyst and TOC analysis of the condensates after the experiments in order to close the carbon  
 218 balance over full cycles of reduction/steam reforming stages under acetic acid and steam feed,  
 219 alternating with the oxidation stage under air feed. A value of X<sub>HAc</sub> during HAc/steam feed lower  
 220 than 100% denoted carbon deposition on the catalyst or in the condensate. The hydrogen yield  
 221 (wt. %) under HAc/steam feed is defined as a ratio of the weight of hydrogen in the process output  
 222 to the weight of acetic acid feedstock (no water) (Equation 2). According to stoichiometry of  
 223 reaction 2, the maximum theoretical hydrogen yield is 13.45 wt%. The hydrogen purity dry basis  
 224 (%) was also calculated as indicated in Equation 3; the water conversion, hydrogen yield and

225 hydrogen purity is compared with chemical equilibrium and stoichiometric values to ascertain the  
 226 efficiency of the fuel-water feed stage.

227 **Equation 2 Hydrogen yield (wt.%)**

$$228 \quad \text{Hydrogen yield (wt. \%)} = \frac{W_{H_2} \times 100 \times \dot{n}_{out,dry} \times y_{H_2}}{W_{HAC} \times n_{HAC,in}}$$

$$229 \quad = \frac{2 \times 1.01 \times 100 \times \dot{n}_{out,dry} \times y_{H_2}}{n_{HAC,in} \times W_{HAC,dry}}$$

230 **Equation 3 Hydrogen Purity (% Dry basis)**

$$231 \quad \text{Hydrogen Purity (\% Dry basis)} = \frac{\text{moles of hydrogen detected in process gas output}}{\text{total gas moles detected} - \text{moles of } N_2} \times 100$$

232 Selectivity to carbon gases and hydrogen gases was also calculated as described in Equation 4 and  
 233 Equation 5 respectively;

234 **Equation 4 Selectivity to C-gases**

$$235 \quad sel_{i,C} \% = 100 \times \frac{\alpha_i y_{i,C}}{\sum_j^n \alpha_j y_{j,C}}$$

236 Where indices  $\alpha_i$  and  $\alpha_j$  represent the carbon atom number of the relevant carbon gas species.

237 **Equation 5 Selectivity to H<sub>2</sub>-gases**

$$238 \quad sel_{i,H_2} \% = 100 \times \frac{\alpha_i y_{i,H_2}}{\sum_j^n \alpha_j y_{j,H_2}}$$

239 Where indices  $\alpha_i$  and  $\alpha_j$  represent the hydrogen atom number of the relevant hydrogen gas species..

240 In the oxidation step, the calculated molar flow rate ( $\dot{n}_{out,dry}$ ) realised from nitrogen balance was  
 241 used to calculate the rate of oxidation of the reduced catalyst ( $\dot{n}_{Ni \rightarrow NiO}$ ) and carbon deposited  
 242 from the prior steam reforming phase ( $\dot{n}_{c,gas}$ ) using an oxygen balance and carbon balance  
 243 respectively as detailed in Equation 6; the integration of the calculated rate over time gave the total  
 244 number of moles of nickel oxidised ( $n_{Ni,t}$ ) and carbon gasified ( $n_{c,gas}$ ) in the oxidation step  
 245 respectively.

246 **Equation 6 Rate of oxidation of reduced nickel catalyst and Carbon gasified**

$$247 \quad (\dot{n}_{Ni \rightarrow NiO}) = 2\dot{n}_{O_2,in} - \dot{n}_{out,dry} \times (2y_{O_2} + y_{CO} + 2y_{CO_2})$$

$$248 \quad (\dot{n}_{c,gas}) = \dot{n}_{out,dry} \times (y_{CO} + y_{CO_2})$$

249 The calculated  $n_{Ni,t}$  was used for the calculation of the extent of nickel conversion using Equation  
 250 7 while the  $n_{c,gas}$  was essential for ascertaining the overall carbon balance of the process and  
 251 extrapolating the extent of carbon gasified (number of moles of carbon gasified at a time with  
 252 respect to the total number of moles gasified at the air feed stage);

253 **Equation 7 Extent of Nickel Oxidation**

254 
$$X_{Ni \rightarrow NiO} (\%) = \frac{n_{Ni,t}}{n_{Ni(i)}} \times 100$$

255 Chemical equilibrium calculations for the parameters considered were determined using values  
256 obtained from the Chemical Equilibrium with Applications (CEA) software [36]. The software  
257 was used to derive equilibrium values for the process output using the set conditions for the  
258 experimental runs (P=1 bar, T= 600°C, 650 °C, Omit= C(gr), H<sub>2</sub>O(cr) H<sub>2</sub>O(l)). These process  
259 outputs were in turn used to calculate the process outputs at equilibrium using Equation 1-  
260 Equation 4 by replacing the relevant molar flow rates in the reactor with just molar outputs  
261 predicted at equilibrium at same conditions.

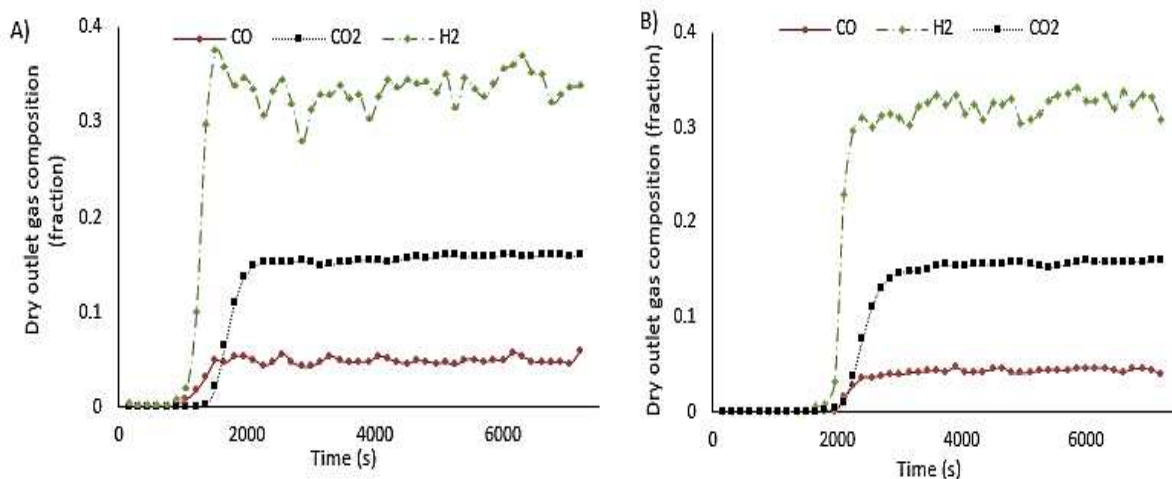
## 262 **3 Results and Discussion**

### 263 **3.1 Process Outputs with time on stream and upon redox cycling of CLSR-HAc**

264 The gases detected by the micro-GC for all experimental runs in this study were CO, CO<sub>2</sub>, CH<sub>4</sub>,  
265 C<sub>2</sub>H<sub>6</sub>, C<sub>3</sub>H<sub>8</sub>, (the last two always remaining below threshold of detection), H<sub>2</sub>, N<sub>2</sub>, and O<sub>2</sub>  
266 (observed during the oxidation steps). In the event of acetone being a significant product of the  
267 process, it would have been detected by significant C content in the condensates. Ketonisation  
268 reactions are generally inhibited by nickel catalysts and are stipulated to occur during the  
269 reforming of acetic acid ideally at temperatures below 600°C [37, 38].

#### 270 **3.1.1 Process Outputs with time on stream- Fuel-Water feed stage**

271 The fuel-steam feed stage as described in 2.2, was carried out at 600°C and 650°C for all  
272 experimental runs in this study. A similar trend for the main output gas species molar fractions  
273 with time on stream was observed for the first cycle (H<sub>2</sub> reduced catalyst) and subsequent cycles  
274 (auto-reduced) for the experimental runs as shown in Figure 2 for catalyst B (T<sub>SR</sub> =600°C, T<sub>OX</sub>  
275 =600°C, S/C= 3, WHSV = 2.5hr<sup>-1</sup>).



276

277 **Figure 2** Dry outlet gas composition of products after reforming at (A) cycle one where the catalyst has been activated by  
 278 reduction with hydrogen (b) Auto reduced catalyst (i.e. catalyst reduced with acetic acid) at the 5th reduction run ( $T_{SR}=$   
 279  $600\text{ }^{\circ}\text{C}$ ,  $T_{Ox}=600\text{ }^{\circ}\text{C}$ , catalyst B,  $WHSV=2.5\text{ hr}^{-1}$ ,  $S/C=3$ )

280 In the  $H_2$  reduced cycle, CO is detected ca. 500 s earlier than  $CO_2$  whereas, in the auto-reduced  
 281 cycle, CO and  $CO_2$  are simultaneously detected. Similarly, the lag between  $H_2$  and CO generation  
 282 is increased by 250 s for the auto-reduced cycle. This is consistent with a steam reforming reaction  
 283 delayed by the consumption of the fuel to carry out the reduction of the nickel oxide to metallic  
 284 nickel, with the steam reactant exhibiting temporary faster reactivity for dissociation to hydrogen  
 285 on the reduced catalyst compared to the hydrocarbon reducing reactions and steam reforming. This  
 286 has also been observed in previous studies where a short lag period or simultaneous partial auto  
 287 reduction and reforming reactions are observed [27, 30]. A similar dry outlet gas composition  
 288 profile was derived for the  $H_2$  reduced cycle and auto reduced cycle when catalyst A was utilised  
 289 with a slight increase in the lag (50s – 200s) between CO and  $H_2$  generation in the auto reduced  
 290 cycle.

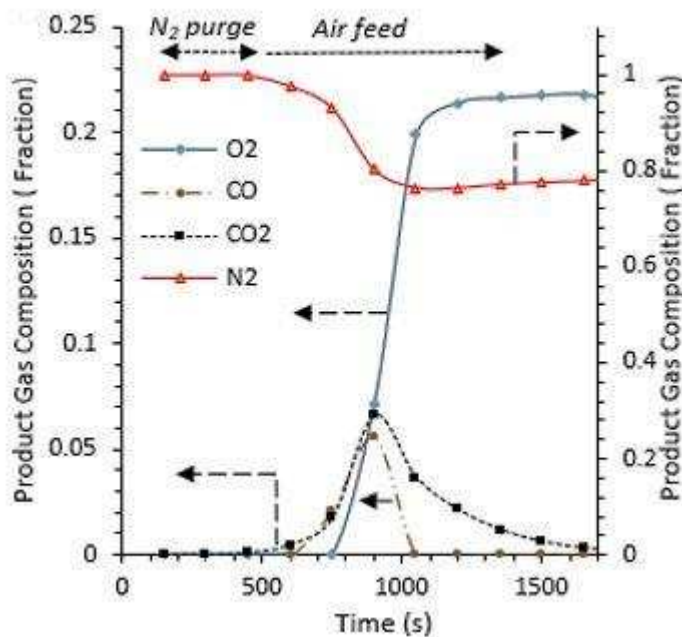
### 291 3.1.2 Process gas Output (Oxidation Phase) and extent of oxidation

292 The oxidation phase in this study was carried out between  $600^{\circ}\text{C}$  and  $800^{\circ}\text{C}$  by passing air through  
 293 the reactor. An increase of approximately  $30\text{--}50^{\circ}\text{C}$  was observed at the beginning of all oxidation  
 294 phase runs; this was due to the exothermic nature of the oxidation reactions.

295 The operating conditions at which the oxidation phase is conducted has an effect on the overall  
 296 process efficiency; it is also fitting to check the extent of oxidation of nickel during the air feed  
 297 stage with the view to ascertain the effectiveness of the air feed stage. Five CLSR cycles (4  
 298 oxidation phase runs) were conducted on catalyst B at  $WHSV\ 1.18\text{ hr}^{-1}$  and at  $S/C$  of 3 to check  
 299 the oxidation effectiveness. Air was passed at 200 sccm and 2g of inert material (sand) were mixed  
 300 with catalyst B (2g) in the reactor load. The oxidation temperature ( $T_{Ox}$ ) under air feed was also

301 set at 800°C while the reducing-steam reforming stage under acetic acid/steam feed was carried  
302 out at 650°C.

303 The process gas composition detected by the micro GC for all oxidation runs under air feed  
304 contained oxygen, nitrogen, CO and CO<sub>2</sub> as depicted in Figure 3. The CO and CO<sub>2</sub> indicate the  
305 oxygen passed through air was utilised in oxidation of carbon that had been formed during the  
306 preceding fuel-steam feed stage; it is also expected as reported in several literature on CLSR that  
307 the catalyst is oxidised from its catalytically active nickel state to deactivated nickel oxide  
308 (reaction 4)[30, 35].



309

310 **Figure 3: Product gas composition (mol fractions) for oxidation step at  $T_{SR}= 650$  °C,  $T_{OX} =800$  °C, catalyst B,**  
311 **WHSV=1.18 hr<sup>-1</sup>, S/C=3, A)**

312 Review of the literature indicates that the oxidation of carbon may occur first before the diffusion  
313 controlled nickel oxidation [35, 39]; however, it was observed in this study that both reactions  
314 occurred in parallel with carbon oxidation starting first and freeing up space on the nickel catalyst  
315 which is then oxidised whilst more carbon is burnt off.

316 Integrating the rates of the nickel oxidation ( $\dot{n}_{Ni \rightarrow NiO}$ ) over time allows to determine whether the  
317 nickel redox extent ( $X_{Ni \rightarrow NiO}$ ) calculated using Equation 7 is maintained at the same level from cycle  
318 to cycle.

319

320 **Table 1 Nickel oxidised in CLSR oxidation phase ( $T_{SR}=650\text{ }^{\circ}\text{C}$ ,  $T_{OX}=800\text{ }^{\circ}\text{C}$ , catalyst B,  $WHSV=1.18\text{ hr}^{-1}$ ,  $S/C=3$ )**

	$\dot{n}_{Ni \rightarrow NiO}$ (mol/s)	$n_{Ni,t}$ (mol)	$X_{Ni \rightarrow NiO}$ (%) (Equation 7)	Duration of Ni Oxidation (s)
<b>1</b>	$8.98 \times 10^{-6}$	$4.03 \times 10^{-3}$	100.22	449
<b>2</b>	$5.99 \times 10^{-6}$	$3.80 \times 10^{-3}$	94.63	634
<b>3</b>	$5.83 \times 10^{-6}$	$3.25 \times 10^{-3}$	80.83	557
<b>4</b>	$6.29 \times 10^{-6}$	$3.37 \times 10^{-3}$	83.97	536

321 The number of moles of nickel oxidised at steady oxygen output (evidencing the end of oxidation  
 322 reactions) is shown in Table 1. There is a drop in the extent of nickel oxidised from the first  
 323 oxidation cycle to subsequent oxidation cycles. However, the extent of nickel oxidation remained  
 324  $>80\%$  across the other cycles; this indicates that the oxidation of nickel can be maintained across  
 325 the oxidation cycles.

### 326 3.1.3 Overall Carbon balance of CLSR process

327 An overall carbon balance was carried out on the CLSR process (using the set operating conditions  
 328 as descibed in 3.1.2) as detailed in Table 2.  $< 5\%$  of the carbon calculated through the carbon  
 329 balance was unaccounted for in the overall process across 5 cycles, indicating high accuracy of  
 330 the carbon balance and distribution across products for the 5 cycles, as well as validating the  
 331 methodology for their calculation.

332 **Table 2:Overall Carbon balance of CLSR process ( $T_{SR}=650\text{ }^{\circ}\text{C}$ ,  $T_{OX}=800\text{ }^{\circ}\text{C}$ , catalyst B,  $WHSV=1.18\text{ hr}^{-1}$ ,  $S/C=3$ )**

	C in feed (mol) during HAC/steam feed	$X_{HAc}$ (%) (Equation 1)	C product during HAC/steam feed (mol)	$n_{Cgas}$ (mol) (Equation 6)	C in the condensate (mol)	Total carbon (gas + solid + condensate) (mol)
1	$6.82 \times 10^{-2}$	93.1	$6.35 \times 10^{-2}$	$5.04 \times 10^{-3}$	$1.99 \times 10^{-5}$	$6.86 \times 10^{-2}$
2	$6.82 \times 10^{-2}$	85.9	$5.86 \times 10^{-2}$	$6.19 \times 10^{-3}$	$4.48 \times 10^{-5}$	$6.49 \times 10^{-2}$
3	$6.82 \times 10^{-2}$	85.7	$5.86 \times 10^{-2}$	$9.64 \times 10^{-3}$	$3.39 \times 10^{-5}$	$6.83 \times 10^{-2}$
4	$6.82 \times 10^{-2}$	91.8	$6.26 \times 10^{-2}$	$7.19 \times 10^{-3}$	$1.39 \times 10^{-5}$	$6.98 \times 10^{-2}$
5	$6.82 \times 10^{-2}$	84.5	$5.76 \times 10^{-2}$	$7.91 \times 10^{-3}$	$0.10 \times 10^{-5}$	$6.55 \times 10^{-2}$

333 The carbon distribution in the products across the process cycles indicates the major share of  
 334 carbon was in the process gas (85%-92%) and as a solid on the oxidised catalyst (7% -14%) across  
 335 all cycles, where  $n_{Cgas}$  represented deposited solid carbon from the previous cycle; these entail  
 336 that most of the carbon in the feedstock was utilised in the process for auto-reduction and steam

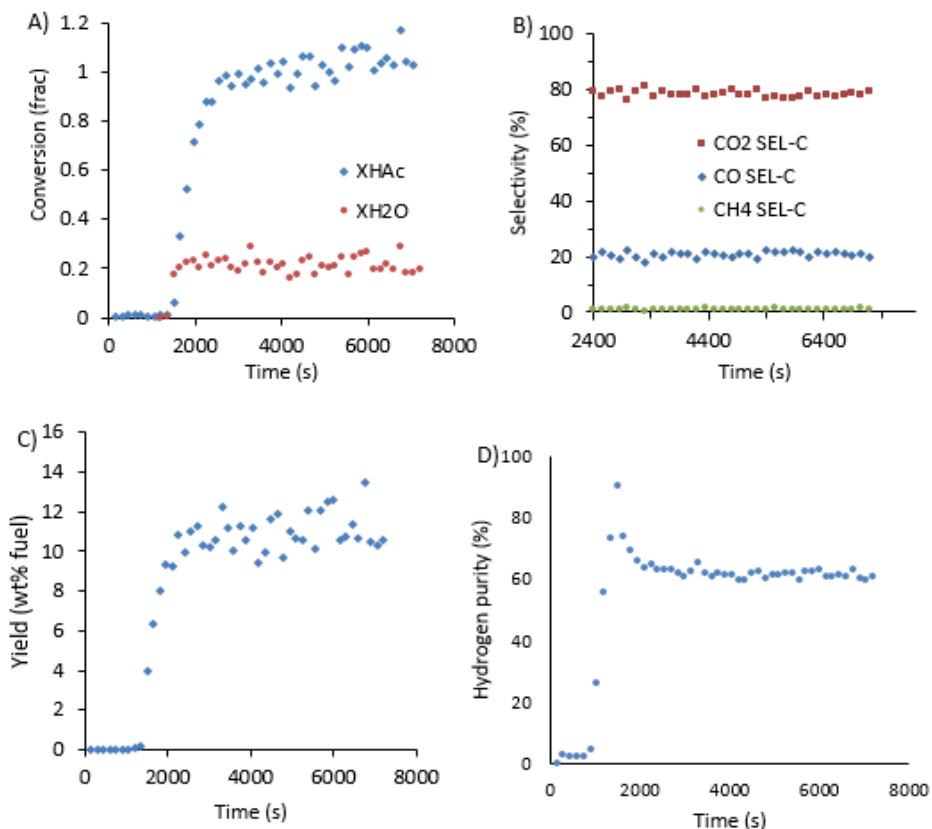
337 reforming, whilst approximately 10% was deposited on the catalyst; it is essential to stress that  
338 the amount deposited on the catalyst must have been influenced by the presence of catalytically  
339 inactive material in the reactor load. Carbon in the condensates was negligible in all the cases.

### 340 **3.2 Effect of oxidation temperature on process outputs**

341 The effect of  $T_{OX}$  on chemical looping steam reforming was investigated by oxidising the used  
342 reforming catalyst (catalyst A) at 600°C, 700°C, and 800°C.  $T_{SR}$  was kept at 600°C and the  
343 experiments were carried out at S/C of 3 and WHSV of 2.36 hr<sup>-1</sup>. The effect of the catalyst utilised  
344 was also investigated by performing 5 reforming experimental cycles using catalyst B at the same  
345 operating conditions but oxidising only at 600°C.

#### 346 **3.2.1 Gas outputs in oxidation temperature study**

347 Both catalysts behaved similarly and efficiently during steam reforming with hydrogen yield  
348 efficiency >83%, hydrogen purity efficiency >97%, water conversion efficiency >75% and fuel  
349 conversion efficiency >89% when compared to equilibrium values. The high efficiency did not  
350 persist to the 2<sup>nd</sup> chemical looping reforming cycle after oxidation was carried out at 600°C for  
351 catalyst A, as sustained reforming could not be maintained over the duration observed. This was  
352 not the case with catalyst B, as sustained production of hydrogen with high efficiency was  
353 observed over five cycles of CLSR with  $T_{OX}$  set to 600°C. The lack of sustained steam reforming  
354 in the second cycle of reforming for catalyst A is due to increased coking via thermal  
355 decomposition (shown in the carbon balances); Coking might have been enhanced by the acidic  
356 nature of the catalyst support in Catalyst A [21, 40, 41]. Acidic catalysts support increases the  
357 chances of thermal decomposition and other polymerisation reactions resulting in graphitic carbon  
358 decomposition on the acidic sites of the support[21].



359

360 **Figure 4 A) Conversion fraction, B) selectivity to C gases, C) hydrogen yield D) hydrogen purity ( $T_{SR} = 600\text{ }^{\circ}\text{C}$ ,  $T_{OX} = 700\text{ }^{\circ}\text{C}$ ,**  
 361 **cycle 2, Catalyst A, WHSV set to 2.36 hr<sup>-1</sup>, and S/C = 3)**

362 Sustained steam reforming was observed during the CLSR of acetic acid using catalyst A after  
 363 oxidising at higher temperatures (700 °C and 800 °C) while leaving the temperature at the reducing  
 364 phase at 600 °C over five cycles (Table 3) Figure 4 shows the conversion fraction, selectivity to  
 365 C gases, hydrogen yield and purity obtained for the duration of the steam reforming phase using  
 366 the auto reduced catalyst A at the second cycle at  $T_{OX}$  set to 700 °C. A similar profile to Figure 4  
 367 was obtained for other cycles at  $T_{OX}$  set to 700 °C or 800 °C. More than 89 % of the fuel was  
 368 converted across all five cycles of CLSR when  $T_{OX}$  was set at 700 °C or 800 °C, corresponding to  
 369 a water conversion efficiency > 73% across all the cycles. This also corresponded to hydrogen  
 370 yield efficiencies > 71% and > 82% when compared to equilibrium and stoichiometric values  
 371 respectively. High hydrogen purity efficiencies (> 97% when compared to equilibrium values and  
 372 > 91% when compared to stoichiometric calculations) were achieved across all CLSR  
 373 experimental runs as shown in Table 3.

374

375

376



	Cycle	$X_{HAc}$ (fraction)			$X_{H_2O}$ (fraction)			Hydrogen purity (%)			Hydrogen yield (wt. %)		
		(Equation 1)						(Equation 3)			(Equation 2)		
$T_{OX}$ ( $^{\circ}\text{C}$ )		600	700	800	600	700	800	600	700	800	600	700	800
Catalyst		B	A		B	A		B	A		B	A	
Reduced by Hydrogen	1	1.02	0.89	0.96	0.21	0.18	0.21	61.09	60.94	61.92	10.80	9.51	10.50
Auto-reduced	2	1.01	0.90	1.00	0.22	0.19	0.21	61.79	61.86	61.55	10.98	9.80	10.72
	3	1.01	0.94	1.01	0.21	0.20	0.24	61.49	61.55	62.87	10.86	10.11	11.48
	4	1.01	1.00	1.06	0.21	0.21	0.23	61.35	61.46	61.74	10.77	10.80	11.63
	5	0.99	1.05	1.07	0.22	0.22	0.23	61.86	61.58	61.66	10.85	11.31	11.64
Equilibrium values		1.00			0.24			63.01			11.47		

378 Thus,  $T_{OX}$  has a bearing effect on the process stability at the subsequent auto-reduction and steam  
 379 reforming run as seen in catalyst A; however, the catalyst support in the catalyst utilised for the  
 380 CLSR process is also essential.

### 381 3.2.2 Solid carbon product in $T_{OX}$ study

382 There is an obvious decline in the carbon content (mol) of catalyst A as  $T_{OX}$  of catalyst A is  
 383 increased as shown in Table 4; with a 68 % decrease in carbon content (mol) found for catalyst A  
 384 when oxidised at  $800\text{ }^{\circ}\text{C}$  compared to  $600\text{ }^{\circ}\text{C}$ . There is also a large difference in the carbon content  
 385 (mol) when catalyst A and catalyst B are compared; the carbon present in catalyst A is much higher  
 386 than that observed in catalyst B when oxidised at  $600\text{ }^{\circ}\text{C}$  (57% increase). CHN analysis of used  
 387 CLSR catalyst A after five cycles of CLSR also exhibits a higher carbon content when compared  
 388 to the corresponding carbon content for catalyst B as seen in Table 4.

389 **Table 4 Solid carbon (CHN elemental analysis) on catalysts A and B at different oxidation temperatures ( $T_{SR} = 600\text{ }^{\circ}\text{C}$ ,  
 390 WHSV= $2.36\text{ hr}^{-1}$ , S/C=3), duration of reforming experiments: 2 hrs in all cases).**

Catalyst, final state, cycle number	$T_{OX}$ ( $^{\circ}\text{C}$ )	$C_{(S)}$ on catalyst (mol)	$C_{(S)}$ on catalyst (mol% of feed C of individual cycle)
Used catalyst B, oxidised, 5 cycles	600	$3.57 \times 10^{-4}$	0.52
Used catalyst A, oxidised, 5 cycles	600	$8.32 \times 10^{-4}$	1.22
Used catalyst A, oxidised, 5 cycles	700	$3.65 \times 10^{-4}$	0.54
Used catalyst A, oxidised, 5 cycles	800	$2.68 \times 10^{-4}$	0.39
Used catalyst B, reduced, 5 cycles	800	$55.6 \times 10^{-4}$	8.15
Used catalyst A, reduced, 5 cycles	800	$79.1 \times 10^{-4}$	11.6

391 The increase in  $T_{OX}$  alone does not alleviate all challenges highlighted in catalyst A because  
 392 incomplete gasification of the carbon deposited in the acidic sites might subsequently occur during  
 393 the oxidation stage, which would prompt further gasification required in the next reforming or  
 394 reducing cycle. This phenomenon would affect the efficiency of the CLSR process as the potential  
 395 of thermal decomposition and cracking reactions might increase particularly at the beginning of

396 the reducing phase where auto-reduction or dominant auto-reduction plus suppressed steam  
 397 reforming are occurring [29, 30].

398 The presence of an alkali support as in the case of catalyst B has been shown to improve the  
 399 stability and selectivity of steam reforming catalysts [42]; they are promoted to increase the  
 400 reforming process by enhancing water gas shift and catalyst reduction [43]. It has also been  
 401 reported that catalysts with less acidic supports such as catalyst B would have a higher ability to  
 402 promote gasification and complete oxidation of deposited carbon, and hence promotes a better  
 403 efficiency for auto-reduction and reforming in subsequent reducing phase [44].

### 404 3.2.3 Catalysts characteristics after CLSR-HAc use in T<sub>OX</sub> study

405 Surface area analysis of the catalysts is also important as it has been associated with the efficiency  
 406 of the reforming process; the surface area analysis of CLSR is difficult to elucidate due to the  
 407 several reactions occurring at the same time, it has been reported that the reduced catalyst (after  
 408 reforming in a looping cycle) would have a higher surface area than its subsequent oxidised form  
 409 [23, 26]. The increase in the surface area and pore volume in the reduced catalysts is due to the  
 410 formation of smaller pores caused by openings of the pore mouths plugged with the oxidised form  
 411 of the catalyst and/or the different molar volume of the Ni particle when compared to its oxidised  
 412 form. Table 5 details results from the BET analysis of catalyst B before and after CLSR (5 cycles,  
 413 S/C=3, T<sub>SR</sub> = 600 °C, WHSV = 2.5 hr<sup>-1</sup>); a loss of surface area and an increase in porosity was  
 414 observed during catalyst activation and reduction using hydrogen. Nevertheless, comparison of  
 415 the used reduced catalyst after several cycles indicates a higher surface area and pore volume in  
 416 the reduced used catalysts when compared to the used oxidised catalyst.

417 **Table 5 BET surface analysis of fresh and used catalyst for CLSR process (S/C=3, T<sub>SR</sub> = 600 °C, WHSV=2.5 hr<sup>-1</sup>)**

	<b>MBET surface area (m<sup>2</sup>/g)</b>	<b>Pore volume (cc/g)</b>	<b>Pore radius (nm)</b>
Fresh Catalyst B (oxidised form)	34.9	0.068	1.9
H <sub>2</sub> -Reduced fresh catalyst	28.8	0.114	2.4
Used oxidised Catalyst B (oxidised at 600 °C after 1 cycle)	20.9	0.084	1.9
Used oxidised catalyst B (oxidised at 800 °C after 1 cycle)	8.6	0.058	1.9
Used reduced Catalyst after 5 cycles of CLSR with oxidation carried out at 600 °C	26.5	0.131	1.9
Used reduced Catalyst after 5 cycles of CLSR with oxidation carried out at 800 °C	13.9	0.072	1.9

418 In regards to oxidation of the catalysts, it was observed that the effect of sintering during oxidation  
 419 is dependent on the temperature of oxidation; higher temperature of oxidation leads to higher level

420 of sintering and a further loss in surface area and open porosity, as observed in Table 5. It can be  
421 postulated that two major phases of surface area changes would occur during the oxidation step,  
422 an increase of surface area and porosity would be achieved due to the opening of pores blocked  
423 by carbon deposition from the subsequent reforming step, followed by a more pronounced  
424 reduction of porosity due to the oxidation of Ni to NiO and resulting sintering particularly at higher  
425 oxidation temperature. It is nevertheless reported that the overall surface area and porosity of the  
426 chemical looping catalyst is expected to stabilise due to the Red-Ox cycle of chemical looping  
427 reforming [23].

428 It is important to note, the consistent and stable profile with time on stream observed in the CLSR  
429 using catalyst B even after oxidation is carried out at 600 °C (Fig. 2) means that acetic acid  
430 decomposition to solid carbon and subsequent carbon gasification reactions are suppressed and  
431 minimised due to its non-acidic support and higher surface area compared to catalyst A. As already  
432 discussed, acidic supports increase the chances of sintering, cracking reactions, thermal  
433 decomposition and other polymerisation reactions which would naturally result to more graphitic  
434 carbon deposition and eventually the deactivation of the catalyst [21, 40]. The graphitic carbon  
435 deposited on the acidic sites of the support of the steam reforming catalyst would be more  
436 prominent in the reforming of feedstocks susceptible to coking and thermal decomposition like  
437 acetic acid. Oxidation of the carbon formed would be more difficult when compared to those  
438 formed on the surface of the catalyst. As seen in the case of catalyst A, this could be improved by  
439 the increase in the temperature of oxidation.

### 440 **3.3 Optimised chemical looping cycling stability for catalyst B at $T_{SR}$ 650 °C and $T_{OX}$** 441 **800°C**

442 Ten CLSR cycles were conducted at 650 °C ( $T_{SR}$ ) using catalyst B, which, as promoted in the  
443 previous section, is a more effective chemical looping reforming catalyst of acetic acid when  
444 compared to catalyst A; these were done at a WHSV of 2.5 hr<sup>-1</sup> and  $T_{OX}$  set to 800 °C.

#### 445 3.3.1 Gas outputs in CLSR cycling stability study

446 A similar product gas profile as identified in Figure 2 with hydrogen, CO, CO<sub>2</sub> and CH<sub>4</sub> as the  
447 main product was observed in all CLSR runs, while in the oxidation run O<sub>2</sub>, CO and CO<sub>2</sub> were the  
448 major products. Table 6 shows the results derived from elemental analysis during the fuel on feed  
449 stage; the conversion fraction ( $X_{HAc}$  and  $X_{H2O}$ ) calculated using Equation 1, hydrogen yield (wt. %)   
450 calculated using Equation 2 and hydrogen purity (%) calculated using Equation 3 were consistent  
451 over the 10 cycles of CLSR, these indicated no obvious loss in the catalyst activity down to coking

452 or catalyst deactivation. The minimum water conversion efficiency when compared to equilibrium  
 453 was 83% with the maximum efficiency at the 9<sup>th</sup> reforming cycle of 92% when compared to  
 454 equilibrium values. The water conversion fraction increased as the fuel conversion increased, but  
 455 no obvious trend which might indicate catalyst deterioration was observed in all 10 CLSR cycles;  
 456 this entails that stable steam reforming with high affinity towards the production of hydrogen was  
 457 apparent in all 10 CLSR cycles. The ‘space time hydrogen yield’, calculated as the moles of  
 458 hydrogen produced per unit mass of catalyst and per unit time was also calculated and shown in  
 459 Table 6. The catalysts auto-reduced by acetic acid performed favourably ( $X_{HAc} > 0.94$ ) when  
 460 compared with the H<sub>2</sub>-reduced catalyst..

461 **Table 6 Acetic acid and water conversion Fractions, hydrogen purity and hydrogen yield (wt.%) ( $T_{SR} = 650$  °C,  $T_{OX} = 800$**   
 462 **°C, catalyst B,  $WHSV = 2.5$  hr<sup>-1</sup>,  $S/C = 3$ )**

	Cycle	$X_{HAc}$	$X_{H_2O}$	Hydrogen purity (%)	Hydrogen yield (wt. %)	Space time yield (mol kg <sub>cat</sub> <sup>-1</sup> h <sup>-1</sup> )
		(Equation 1)		(Equation 3)	(Equation 2)	
H <sub>2</sub> -Reduced	1	1.00	0.21	61.77	10.92	27.75
Auto- reduced	2	0.95	0.20	61.71	10.31	26.20
	3	0.98	0.20	61.63	10.56	26.85
	4	0.98	0.21	62.04	10.75	27.30
	5	0.97	0.20	61.73	10.52	26.75
	6	0.98	0.20	61.69	10.63	27.00
	7	0.96	0.21	61.99	10.51	26.70
	8	0.95	0.20	61.87	10.40	26.40
	9	1.05	0.22	61.88	11.38	28.95
	10	1.03	0.22	61.90	11.23	28.55
	Equilibrium	1.00	0.24	63.14	11.53	

463 This is similar to previous studies on chemical looping steam reforming of pyrolysis oils, which  
 464 concluded that auto-reduction of acetic acid and subsequent reforming of acetic acid and pyrolysis  
 465 oil can be done efficiently without obvious deterioration in its feedstock conversion [28, 30].

466 The hydrogen yield (wt. %) and the purity of hydrogen (% dry basis) produced also showed high  
 467 stability across all cycles; the efficiency of the yield across all 10 cycles of chemical looping  
 468 reforming was between 89% and 97% when compared to equilibrium, and 77% and 85% when  
 469 compared to theoretical maximum. The trend in the hydrogen yield also corresponds to the fuel  
 470 conversion ( $X_{HAc}$ ) of the reducing-steam reforming stage. The hydrogen purity (%) was also  
 471 consistent across all 10 cycles in the reducing phase with an efficiency of 93% observed across all  
 472 cycles when compared to equilibrium calculations, this is equivalent to 98% compared to  
 473 theoretical maximum or stoichiometric values.

474 As seen in Table 7, the selectivity to hydrogen containing gases (Sel H<sub>2,H<sub>2</sub></sub> and  
 475 Sel CH<sub>4,H<sub>2</sub></sub>) shows no disparity across all 10 reforming cycles. CH<sub>4</sub> is an intermediate by-product  
 476 formed from methanation reactions (prominent at lower temperatures) and homogenous cracking  
 477 of acetic acid which is promoted on nickel catalysts due to its high affinity towards breaking C-C  
 478 bonds [45-47]; its decomposition has been attributed as one of the major routes of catalyst  
 479 deactivation for the steam reforming of acetic acid [48]. The Sel CH<sub>4,H<sub>2</sub></sub> is primarily determined  
 480 by the S/C, catalyst loading and T<sub>SR</sub>; nevertheless, high selectivity to methane ranging from 4%  
 481 to ca15% has been reported in previous studies on nickel catalysts[49, 50]. The obtained  
 482 Sel CH<sub>4,H<sub>2</sub></sub> and Sel H<sub>2,H<sub>2</sub></sub> in this study are relatively close to equilibrium values and consistent  
 483 across all 10 cycles of CLSR. This strongly indicate, the rate of reaction of the process is primarily  
 484 determined by the thermodynamics of the reaction system. It also indicates, no loss of activity in  
 485 the efficiency of the reforming catalyst towards efficient steam reforming and hydrogen  
 486 production across all 10 cycles of CLSR. In regards to selectivity to C-gases, there is no major  
 487 change identified for selectivity to CH<sub>4,C</sub>.The selectivity to CO<sub>2</sub> increased sparingly from the first  
 488 cycle (H<sub>2</sub>-reduced catalyst) to the subsequent cycles; this also corresponded to a decrease in the  
 489 selectivity to CO from the first cycle to subsequent cycles, for the auto-reduced catalyst. This  
 490 observation coupled with the stable water conversion fraction indicates improved water gas shift  
 491 in the reducing-steam reforming stage and could also indicate less carbon gasification.

492 **Table 7: Selectivity to C-gases and H-gases across 10 cycles (T<sub>SR</sub>= 650 °C, T<sub>OX</sub>=800 °C, catalyst B, WHSV=2.5 hr<sup>-1</sup>,**  
 493 **S/C=3)**

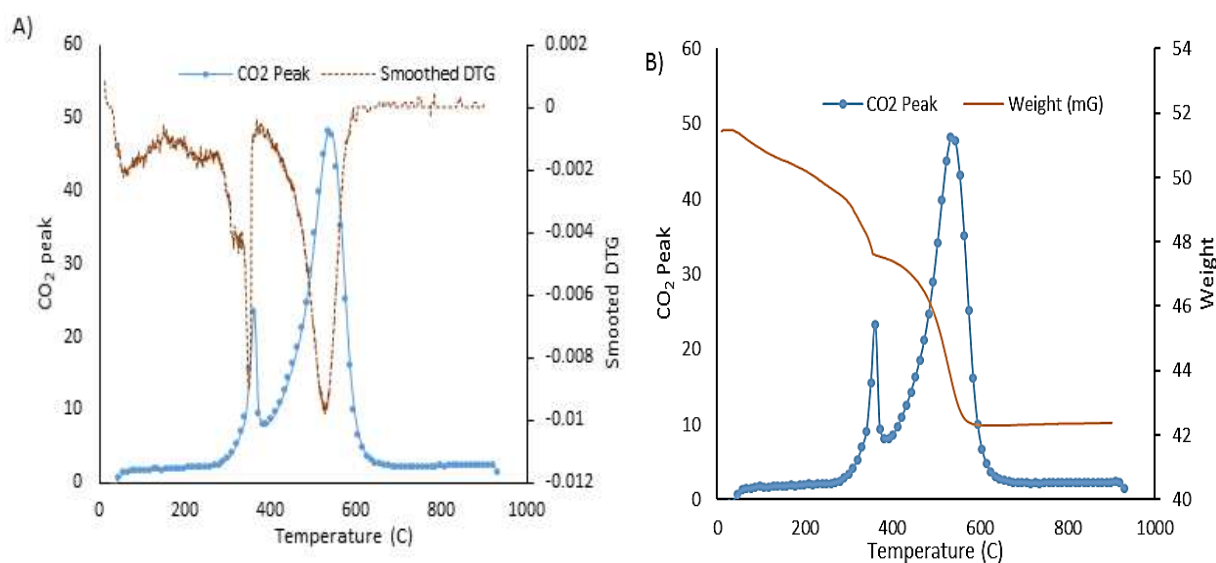
	Cycle	Selectivity to C-gases (Equation 4)			Selectivity to H-gases (Equation 5)	
		Sel CO <sub>2,C</sub>	Sel CO <sub>C</sub>	Sel CH <sub>4,C</sub>	Sel H <sub>2,H<sub>2</sub></sub>	Sel CH <sub>4,H<sub>2</sub></sub>
H <sub>2</sub> -Reduced	1	75.9	23.5	0.6	99.6	0.4
Auto reduced	2	77.6	21.8	0.7	99.6	0.4
	3	77.5	22.0	0.5	99.7	0.3
	4	78.5	20.9	0.5	99.7	0.3
	5	78.4	21.1	0.5	99.7	0.3
	6	77.8	21.7	0.5	99.7	0.3
	7	78.4	21.2	0.4	99.7	0.3
	8	78.2	21.4	0.4	99.8	0.2
	9	78.1	21.4	0.5	99.7	0.3
	10	78.2	21.4	0.5	99.7	0.3
Equilibrium		72.8	26.8	0.4	99.5	0.5

### 494 3.3.2 Solid Carbon Product in Redox cycling stability study

495 Post experimental analysis on the used chemical looping reforming catalyst and condensates  
 496 samples collected over 10 cycles were also conducted; the possibility of leaching of nickel catalyst

497 has been postulated for steam reforming of acetic acid[30], hence to check the extent of leaching,  
498 ICP-MS testing was carried out on the condensate collected after the 10<sup>th</sup> chemical looping cycle.  
499 0.0819 mg/L of nickel was detected through ICP-MS, which indicated potential leaching of the  
500 catalyst into the condensate, these however corresponded to about 0.0001% of the nickel originally  
501 present in the catalyst and is therefore taken as insignificant. Total organic carbon analysis of the  
502 condensates collected after the reducing-steam reforming phase of the CLSR experimental runs  
503 using catalyst B indicates there was no obvious trend or relationship across the cycles. The carbon  
504 (mol) found in the condensate constituted less than 0.1 % of all carbon formed for each  
505 experimental run with the majority share of carbon formed either present in the product gas as  
506 CO<sub>2</sub>, CO and CH<sub>4</sub> formed during oxidation or auto-reduction/reforming or deposited as solid on  
507 the catalyst.

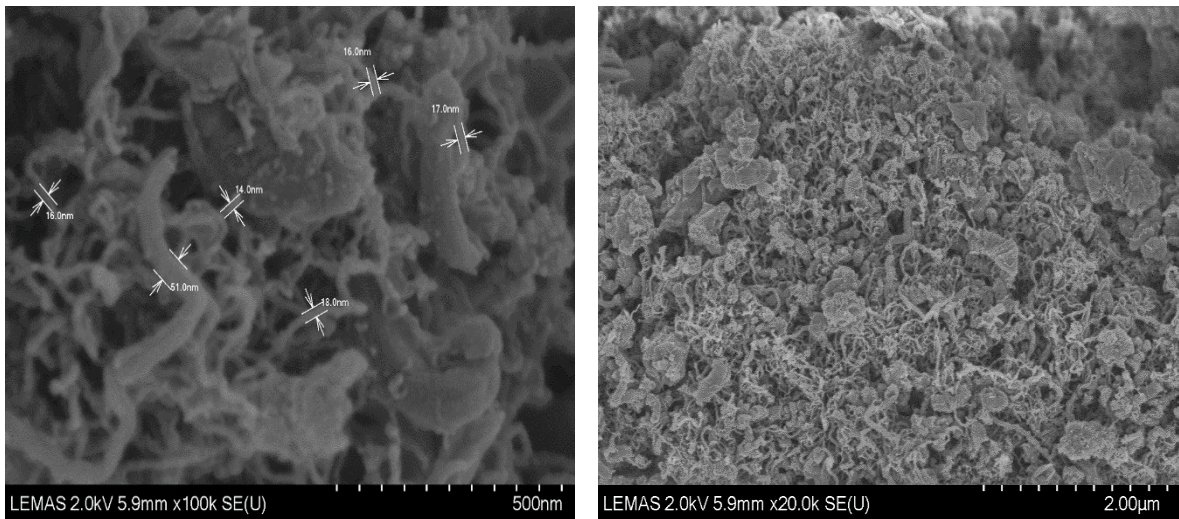
508 TGA-FTIR analysis was conducted on the used, reduced, CLSR catalyst after 10 cycles of  
509 chemical looping steam reforming cycles. The evolution of CO<sub>2</sub> from the FTIR chemigram was  
510 plotted against the weight loss of catalyst from the TGA (Figure 5); Two CO<sub>2</sub> peaks were observed  
511 in the Chemigram profile [30, 48]; this indicates that two forms of carbon were formed. Previous  
512 studies indicate that the CO<sub>2</sub> generated at the lower temperature (360°C) was due to coking on the  
513 active sites of the surface of the catalyst while the other type of carbon formed (544°C) was  
514 pseudo-graphitic in structure and contains poly aromatic compounds. These are most likely formed  
515 in and on the catalyst support or in some cases at the interface between the catalyst supports and  
516 the active sites [21, 30, 51, 52].



517

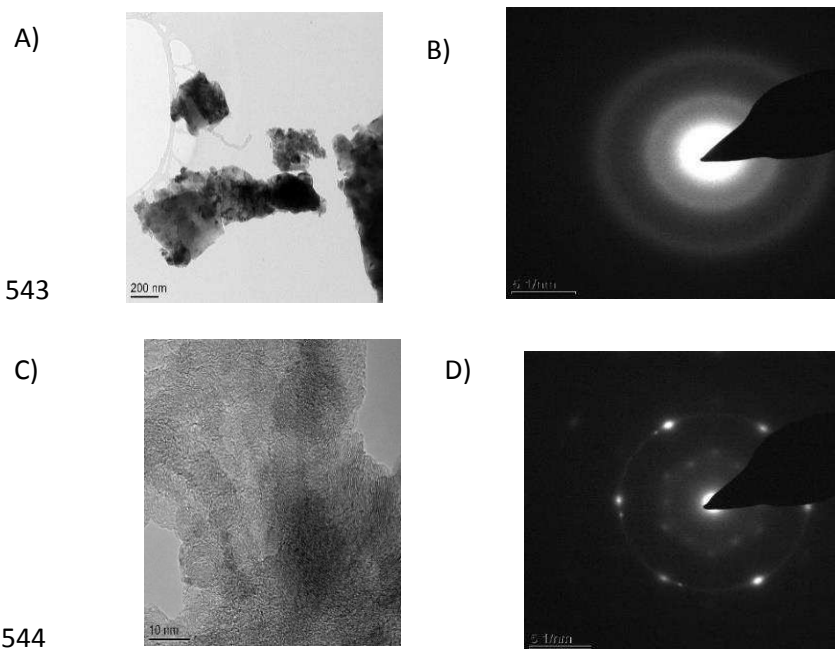
518 **Figure 5: TGA FTIR analysis of used CLSR catalyst B (reduced form) A) CO<sub>2</sub> against smoothed DTG B) CO<sub>2</sub> against**  
519 **weight loss of catalyst (T<sub>SR</sub>=650 °C, T<sub>Ox</sub>=800 °C, S/C= 3 and WHSV=2.36 hr<sup>-1</sup>)**

520 3.3.3 Catalysts characteristics after CLSR-HAc use in Redox stability study  
521 SEM images of the used CLSR catalyst (Figure 6) shows the presence of filamentous carbon; in  
522 higher magnification, it is observed that two types of carbon filaments were formed in regards to  
523 size of the carbon filaments. Denser and larger carbon filaments with a diameter of 51nm were  
524 identified, and shorter and smaller filaments with diameter between 14nm to 18 nm which formed  
525 the major share of carbon filaments were also observed. It has been suggested in a previous study  
526 that the size of the carbon filaments formed on the surface of the catalyst might have an effect on  
527 the process efficiency [30]; the presence of more dense or larger carbon filaments would make it  
528 more difficult for the fuel and steam reacting molecules to reach the active sites of the catalyst  
529 thus introducing a larger external mass transfer barrier and hence reducing the rate of reaction and  
530 catalytic activity. The oxidation of shorter and smaller carbon filaments which are prominent on  
531 catalyst B is also easier when compared to oxidation of larger and denser carbon filaments.



532  
533 **Figure 6: SEM images of the Used CLSR catalyst B after 10 cycles (in reduced form)  $T_{SR}= 650\text{ }^{\circ}\text{C}$ ,  $T_{OX}=800\text{ }^{\circ}\text{C}$ , catalyst**  
534 **B, WHSV=2.5 hr<sup>-1</sup>, S/C=3**

535 TEM images and SAED diffraction patterns of the used CLSR catalyst can be seen in Figure 7;  
536 the images in Figure 7(A) and the diffraction pattern in Figure 7(B) indicate and confirm the  
537 presence of amorphous carbon across the catalyst; these carbon spots are not evenly distributed  
538 across the catalyst but are dispersed. The different intensity in the colours also indicates, the level  
539 of carbon deposition varies across different point of the catalyst. A poly-crystalline structure  
540 Figure 7(C,D) was also observed in higher magnification of the catalyst which as expected  
541 represents the pseudo graphitic carbon formed as already reported for the steam reforming of acetic  
542 acid [30].



545 **Figure 7** TEM images and Diffraction patterns of used chemical looping steam reforming catalysts (in reduced form)  
 546 after 10 cycles of reforming;  $T_{SR}=650\text{ }^{\circ}\text{C}$ ,  $T_{OX}=800\text{ }^{\circ}\text{C}$ , catalyst B,  $WHSV=2.5\text{ hr}^{-1}$ ,  $S/C=3$

547 The poly crystalline structure as observed in the SAED diffraction patterns (Figure 7D)  
 548 corresponds to  $\text{CO}_2$  peak observed at higher temperatures in the chemigram obtained from TGA-  
 549 FTIR analysis as detailed in Figure 5 while the amorphous carbon corresponds to the carbon  
 550 filaments as observed in SEM images (Figure 6) and the lower  $\text{CO}_2$  peak in the TGA-FTIR  
 551 chemigram (Figure 5).

## 552 4 Conclusion

553 An experimental study was performed using two conventional nickel based catalysts in a packed  
 554 bed reactor to study the possibility and efficiency of chemical looping steam reforming of acetic  
 555 acid, as a model compound of pyrolysis oils. The following observations and inferences were  
 556 deduced after post experimental analysis;

- 557 • The temperature at which the catalyst is oxidised in the air feed/ oxidation step plays a  
 558 vital role in chemical looping steam reforming; this is however dependent on the type of  
 559 catalyst utilised;
- 560 • Acetic acid is thermally unstable and decomposes easily; however, chemical looping steam  
 561 reforming process can be sustained at the right operating conditions as gasification of  
 562 carbon deposited occurs as the reaction goes on
- 563 • The auto reduction of the oxidised catalyst by acetic acid in an integrated system can be  
 564 sustained across several cycles at the operating conditions set for this study;



565 • An overall carbon balance also indicated that in the overall cyclic process, the majority of  
566 the carbon from the feedstock is converted efficiently to the product gas with no apparent  
567 loss of activity in the cycles.

568 It can then be concluded that chemical looping steam reforming of acetic acid can be carried  
569 out successfully and efficiently with a high fuel conversion and hydrogen yield across several  
570 cycles at a stable and sustainable rate as long as the operating parameters in regards to catalyst  
571 type, reforming and oxidising temperature, and steam to carbon ratio are taken into account.

## 572 **5 Acknowledgement**

573 The authors would like to acknowledge the Niger Delta Development Commission (NDDC)  
574 Nigeria for financial support. Martyn V. Twigg at TST Limited is gratefully acknowledged for  
575 providing the nickel catalysts. We also thank the UKCCSRC EPSRC consortium  
576 (EP/G01244X/1) for call to grant “SUPERGEN: Delivery of Sustainable Hydrogen”.

## 577 **References**

- 578 [1] PATH, Annual Report on World Progress in Hydrogen, Partnership for Advancing the Transition to  
579 Hydrogen (PATH), Washington, D.C, 2011.
- 580 [2] D.B. Levin, R. Chahine, international journal of hydrogen energy 35 (2010) 4962-4969.
- 581 [3] J. Ritter, A. Ebner, report for US Department of Energy (2005).
- 582 [4] R. Navarro, M. Sanchez-Sanchez, M. Alvarez-Galvan, F. Del Valle, J. Fierro, Energy &  
583 Environmental Science 2 (2009) 35-54.
- 584 [5] C. Zygarlicke, Renewable Hydrogen: Biomass for Sustainable Hydrogen Transportation Fuel,  
585 Biomass Magazine, BBI International, Grand Forks, 2014.
- 586 [6] T.A. Milne, C.C. Elam, R.J. Evans, Hydrogen from Biomass: State of the Art and Research  
587 Challenges, International Energy Agency, USA, 2001.
- 588 [7] M. Balat, Energy Sources, Part A 31 (2009) 516-526.
- 589 [8] X. Hu, G. Lu, Applied Catalysis B: Environmental 88 (2009) 376-385.
- 590 [9] D. Wang, D. Montane, E. Chornet, Applied Catalysis A: General 143 (1996) 245-270.
- 591 [10] C. Rioche, S. Kulkarni, F.C. Meunier, J.P. Breen, R. Burch, Applied Catalysis B: Environmental 61  
592 (2005) 130-139.
- 593 [11] F. Bimbela, M. Oliva, J. Ruiz, L. García, J. Arauzo, Journal of Analytical and Applied Pyrolysis 85  
594 (2009) 204-213.
- 595 [12] F. Bimbela, M. Oliva, J. Ruiz, L. García, J. Arauzo, Journal of analytical and applied pyrolysis 79  
596 (2007) 112-120.
- 597 [13] S. Czernik, R. French, C. Feik, E. Chornet, Industrial & Engineering Chemistry Research 41 (2002)  
598 4209-4215.
- 599 [14] S. Czernik, R. French, C. Feik, E. Chornet, Production of hydrogen from biomass-derived liquids,  
600 DOE Hydrogen Program Review, 2001.
- 601 [15] R.M. Zin, Advanced Steam Reforming of Pyrolysis Oils and their aqueous phase, School of Process,  
602 Environmental and Materials Engineering, University of Leeds, Energy and Research Institute, 2012.
- 603 [16] K. Sipilä, E. Kuoppala, L. Fagernäs, A. Oasmaa, Biomass and Bioenergy 14 (1998) 103-113.
- 604 [17] P. Pimenidou, V. Dupont, Bioresource technology 109 (2012) 198-205.

605 [18] X. Hu, G. Lu, Applied Catalysis B: Environmental 99 (2010) 289-297.  
606 [19] K. Takanahe, K.-i. Aika, K. Seshan, L. Lefferts, Journal of catalysis 227 (2004) 101-108.  
607 [20] K. Takanahe, K.-i. Aika, K. Seshan, L. Lefferts, Chemical Engineering Journal 120 (2006) 133-137.  
608 [21] A. Basagiannis, X. Verykios, Applied Catalysis A: General 308 (2006) 182-193.  
609 [22] V. Dupont, A. Ross, I. Hanley, M. Twigg, International journal of hydrogen energy 32 (2007) 67-  
610 79.  
611 [23] B. Jiang, B. Dou, Y. Song, C. Zhang, B. Du, H. Chen, C. Wang, Y. Xu, Chemical Engineering Journal  
612 280 (2015) 459-467.  
613 [24] Q. Zafar, T. Mattisson, B. Gevert, Industrial & engineering chemistry research 44 (2005) 3485-  
614 3496.  
615 [25] T. Hoang, B. Geerdink, J. Sturm, L. Lefferts, K. Seshan, Applied catalysis B: environmental 163  
616 (2015) 74-82.  
617 [26] N. Giannakeas, A. Lea-Langton, V. Dupont, M.V. Twigg, Applied Catalysis B: Environmental 126  
618 (2012) 249-257.  
619 [27] R.M. Zin, A. Ross, J. Jones, V. Dupont, Bioresource technology 176 (2015) 257-266.  
620 [28] A. Lea-Langton, R.M. Zin, V. Dupont, M.V. Twigg, International Journal of Hydrogen Energy 37  
621 (2012) 2037-2043.  
622 [29] J. Feroso, M.V. Gil, F. Rubiera, D. Chen, ChemSusChem 7 (2014) 3063-3077.  
623 [30] F. Cheng, V. Dupont, International Journal of Hydrogen Energy 38 (2013) 15160-15172.  
624 [31] P.N. Kechagiopoulos, S.S. Voutetakis, A.A. Lemonidou, I.A. Vasalos, Energy & fuels 20 (2006) 2155-  
625 2163.  
626 [32] E.C. Vagia, A.A. Lemonidou, Applied Catalysis A: General 351 (2008) 111-121.  
627 [33] R.M. Zin, A. Lea-Langton, V. Dupont, M.V. Twigg, International Journal of Hydrogen Energy 37  
628 (2012) 10627-10638.  
629 [34] F. Cheng, V. Dupont, M.V. Twigg, Applied Catalysis B: Environmental 200 (2017) 121-132.  
630 [35] P. Pimenidou, G. Rickett, V. Dupont, M. Twigg, Bioresource technology 101 (2010) 6389-6397.  
631 [36] S. Gordon, B.J. McBride, Computer program for calculation of complex chemical equilibrium  
632 compositions and applications, National Aeronautics and Space Administration, Office of Management,  
633 Scientific and Technical Information Program, 1996.  
634 [37] A.A. Lemonidou, E.C. Vagia, J.A. Lercher, ACS Catalysis 3 (2013) 1919-1928.  
635 [38] M.N. Khan, T. Shamim, Energy Procedia 61 (2014) 2034-2037.  
636 [39] P. Pimenidou, Novel Process of Hydrogen Production from Liquids of Biomass Origin, School of  
637 Process, Environmental and Material Engineering, University of Leeds, 2010.  
638 [40] A. Basagiannis, X. Verykios, International journal of hydrogen energy 32 (2007) 3343-3355.  
639 [41] S. Goicoechea, E. Kraveva, S. Sokolov, M. Schneider, M.-M. Pohl, N. Kockmann, H. Ehrich, Applied  
640 Catalysis A: General 514 (2016) 182-191.  
641 [42] J.d.S. Lisboa, D.C. Santos, F.B. Passos, F.B. Noronha, Catalysis today 101 (2005) 15-21.  
642 [43] K. Kousi, N. Chourdakis, H. Matralis, D. Kontarides, C. Papadopoulou, X. Verykios, Applied Catalysis  
643 A: General 518 (2016) 129-141.  
644 [44] V. Nichele, M. Signoretto, F. Pinna, F. Menegazzo, I. Rossetti, G. Cruciani, G. Cerrato, A. Di Michele,  
645 Applied Catalysis B: Environmental 150 (2014) 12-20.  
646 [45] J. Sinfelt, Advances in catalysis 23 (1973) 91-119.  
647 [46] R. Davda, J. Shabaker, G. Huber, R. Cortright, J.A. Dumesic, Applied Catalysis B: Environmental 43  
648 (2003) 13-26.  
649 [47] S.C.M. Mizuno, A.H. Braga, C.E. Hori, J.B.O. Santos, J.M.C. Bueno, Catalysis Today.  
650 [48] W. Nabgan, T.A.T. Abdullah, R. Mat, B. Nabgan, A.A. Jalil, L. Firmansyah, S. Triwahyono,  
651 International Journal of Hydrogen Energy 42 (2017) 8975-8985.  
652 [49] Z. Li, X. Hu, L. Zhang, S. Liu, G. Lu, Applied Catalysis A: General 417 (2012) 281-289.  
653 [50] S. Thairachoenutcharittham, V. Meeyoo, B. Kitiyanan, P. Rangsunvigit, T. Rirksomboon, Catalysis  
654 today 164 (2011) 257-261.

655 [51] D. Duprez, M. Demicheli, P. Marecot, J. Barbier, O. Ferretti, E. Ponzi, *Journal of Catalysis* 124  
656 (1990) 324-335.  
657 [52] J. Barbier, *Applied catalysis* 23 (1986) 225-243.

658

659